communications biology

A Nature Portfolio journal

Article

https://doi.org/10.1038/s42003-025-07921-3

Roles of TLR4 in macrophage immunity and macrophage-pulmonary vascular/lymphatic endothelial cell interactions in sepsis

Yu Fu[1,2,7], Ting Gong[1,3,7], Patricia A. Loughran[1], Yuehua Li[1], Timothy R. Billiar[1,4], Youtan Liu[3], Zongmei Wen[2] & Jie Fan[1,4,5,6]

In sepsis, acute lung injury (ALI) is a severe complication and a leading cause of death, involving complex mechanisms that include cellular and molecular interactions between immune and lung parenchymal cells. In recent decades, the role of Toll-like receptor 4 (TLR4) in mediating infection-induced inflammation has been extensively studied. However, how TLR4 facilitates interactions between innate immune cells and lung parenchymal cells in sepsis remains to be fully understood. This study aims to explore the role of TLR4 in regulating macrophage immunity and metabolism in greater depth. It also seeks to reveal how changes in these processes affect the interaction between macrophages and both pulmonary endothelial cells (ECs) and lymphatic endothelial cells (LECs). Using TLR4 knockout mice and the combined approaches of single-cell RNA sequencing and experimental validation, we demonstrate that in sepsis, TLR4-deficient macrophages upregulate Abca1, enhance cholesterol efflux, and reduce glycolysis, promoting M2 polarization and attenuating inflammation. These metabolic and phenotypic shifts significantly affect their interactions with pulmonary ECs and LECs. Mechanistically, we uncovered that TLR4 operates through multiple pathways in endothelial dysfunction: macrophage TLR4 mediates inflammatory damage to ECs/LECs, while endothelial TLR4 both directly sensitizes cells to lipopolysaccharide-induced injury and determines their susceptibility to macrophage-derived inflammatory signals. These findings reveal the complex role of TLR4 in orchestrating both immune-mediated and direct endothelial responses during sepsis-induced ALI, supporting that targeting TLR4 on multiple cell populations may present an effective therapeutic strategy.

Sepsis represents one of the most challenging critical care conditions worldwide, characterized by life-threatening organ dysfunction resulting from dysregulated host responses to infection[1,2]. Among various organ systems affected during sepsis, the lungs exhibit particular vulnerability to inflammatory injury, frequently manifesting as acute lung injury (ALI) or its more severe form, acute respiratory distress syndrome (ARDS)[3,4]. Despite advances in critical care medicine, including the implementation of lung-protective ventilation strategies, early antimicrobial therapies, and anti-inflammatory medication interventions, the mortality rate for sepsis-induced ALI remains unacceptably high at 30-40%[5–7].

Clinically, sepsis-induced ALI/ARDS manifests as severe hypoxemia and pulmonary leakage, primarily resulting from compromised endothelial barrier function[8,9]. The vascular endothelium, comprising endothelial cells (ECs), forms a dynamic barrier between circulating blood and tissues[10], while lymphatic endothelial cells (LECs) lining the pulmonary lymphatic vessels regulate fluid clearance[11]. The dysfunction of both EC and LEC

[1]Department of Surgery, University of Pittsburgh School of Medicine, Pittsburgh, PA, 15213, USA. [2]Department of Anesthesiology, Shanghai Pulmonary Hospital, School of Medicine, Tongji University, Shanghai, 200433, China. [3]Department of Anesthesiology, Shenzhen Hospital of Southern Medical University, Shenzhen, 518110, China. [4]McGowan Institute for Regenerative Medicine, University of Pittsburgh, Pittsburgh, PA, 15219, USA. [5]Research and Development, Veterans Affairs Pittsburgh Healthcare System, Pittsburgh, PA, 15240, USA. [6]Department of Immunology, University of Pittsburgh School of Medicine, Pittsburgh, PA, 15213, USA. [7]These authors contributed equally: Yu Fu, Ting Gong. e-mail: jif7@pitt.edu

barriers leads to the extravasation of fluid, proteins, and inflammatory cells into the pulmonary interstitium and alveolar spaces[12,13]. This pathological process is exacerbated by complex interactions between ECs/LECs and infiltrating immune cells, contributing to sustained inflammation and tissue damage[14,15]. Therefore, understanding the crosstalk between immune cells and pulmonary ECs/LECs is crucial for elucidating the pathogenesis of sepsis-induced ALI.

In recent decades, Toll-like receptor 4 (TLR4) has been recognized as a pivotal pattern recognition receptor (PRR) that mediates infection-induced inflammation by detecting both pathogen-associated molecular patterns (PAMPs), such as bacterial lipopolysaccharide (LPS), and damage-associated molecular patterns (DAMPs)[16,17]. While TLR4 is predominantly expressed in immune cells, in which TLR4 plays a central role in orchestrating innate immune responses, emerging evidence highlights its substantial expression and function in lung parenchymal cells, particularly ECs[18,19]. Although the role of TLR4 in initiating inflammatory cascades is well-established, its contribution to the intricate interplay between innate immune cells and lung parenchymal cells during sepsis remains to be fully understood. This knowledge gap is particularly significant regarding LECs, a crucial yet understudied cellular component in sepsis-induced ALI.

Single-cell RNA sequencing (scRNA-seq) has emerged as a powerful tool for decoding cellular heterogeneity and intercellular communication. Using TLR4 knockout (*Tlr4*$^{-/-}$) mice combined with scRNA-seq analysis and experimental validation, we investigated the role of TLR4 in sepsis-induced ALI. Our comprehensive analysis revealed that TLR4 deficiency alters macrophage metabolism and phenotype, promoting an anti-inflammatory state characterized by enhanced cholesterol efflux and reduced glycolysis. Furthermore, we uncovered novel mechanisms by which TLR4 orchestrates the complex interactions between macrophages and both ECs and LECs during sepsis. These findings advance our understanding of TLR4's multifaceted role in sepsis-induced ALI and further suggest potential therapeutic strategies targeting TLR4-mediated cellular responses.

Results

Genetic deletion of TLR4 exhibits wide transcriptomic alterations in the lungs following sepsis

To explore the cellular and molecular mechanisms by which TLR4 influences sepsis-induced ALI, we analyzed lung cells from *Tlr4*$^{-/-}$ mice subjected to cecal ligation and puncture (CLP)-induced sepsis at 24 h and sham, integrating publicly available data for wild-type (WT) CLP and sham operation at 24 h from the GEO database (GSE278767)[20]. This combined dataset underwent scRNA-seq analysis to examine the impact of TLR4 deficiency. Following rigorous quality control (Supplementary Fig. 1A–C), a total of 18,152 cells were included in the subsequent analysis. Based on relevant marker genes (Supplementary Fig. 2A), we identified and annotated seven distinct cell populations, including fibroblast, epithelial cell, EC, smooth muscle cell (SMC), myeloid cell, mesothelial cell, and LEC (Fig. 1A). Quantification of these cell types revealed significant differences in myeloid cell and EC populations between the WT CLP and *Tlr4*$^{-/-}$ CLP groups (Supplementary Fig. 2B, C).

Differential expression analysis between the WT CLP and *Tlr4*$^{-/-}$ CLP groups demonstrated distinct transcriptional profiles across various cell types (Fig. 1B). Further examination of gene expression changes identified key pro-inflammatory genes, including *Cxcl13*, *Il1r1*, and *Casp12*, which were significantly upregulated in the WT CLP group compared to *Tlr4*$^{-/-}$ CLP (Fig. 1C). Pathway enrichment analysis of the differentially expressed genes (DEGs) revealed that key pathways associated with inflammation, including cytokine–cytokine receptor interaction, NF-κB signaling, TNF signaling, and neutrophil migration, were significantly upregulated in the WT CLP group, underscoring the pro-inflammatory influence of TLR4 (Fig. 1D).

Together, these findings highlight the significant impact of TLR4 deficiency on the cellular and transcriptional landscape of lung cells during sepsis-induced ALI, particularly in myeloid cells, ECs, and other key cell populations, demonstrating a broad modulation of gene expression in the absence of TLR4.

The phenotypic changes in sepsis-induced lung injury are consistent with the transcriptomic alterations caused by TLR4 deficiency

To investigate the role of TLR4 in ALI, we subjected both WT and *Tlr4*$^{-/-}$ mice to CLP for 24 h and detected TLR4 expression in lung tissue using immunofluorescence staining. TLR4 expression is significantly higher in the WT CLP group than in WT Sham animals (Fig. 2A). In macrophages isolated from the bronchoalveolar lavage fluid (BALF), TLR4 levels were also elevated in the WT CLP group compared to WT Sham (Fig. 2B). Western blot analysis of lung tissues confirmed the upregulation of TLR4 in WT mice after CLP, while no TLR4 expression was detected in *Tlr4*$^{-/-}$ mice, verifying the knockout of TLR4 (Fig. 2C).

The absence of TLR4 was associated with reduced lung injury following CLP. Compared to WT mice, *Tlr4*$^{-/-}$ mice exhibited reduced cellular infiltration, decreased pulmonary edema, and significantly lower lung injury scores (Fig. 2D, E). CLP caused a significant increase in neutrophil recruitment to the alveolar space in WT mice compared to sham controls. In contrast, neutrophil recruitment was markedly reduced in *Tlr4*$^{-/-}$ mice (Fig. 2F). Additionally, quantification of pro-inflammatory cytokines in BALF demonstrated that *Tlr4*$^{-/-}$ mice had significantly lower levels of IL-1β and TNF-α (Fig. 2G, H), indicating an attenuated neutrophil infiltration and inflammatory response in the absence of TLR4.

In terms of capillary barrier function, *Tlr4*$^{-/-}$ mice showed a significant reduction in BALF protein concentration (Fig. 2I), along with a notably lower lung wet-to-dry ratio (Fig. 2J). This was further corroborated by the reduced extravasation of Evans blue dye in the lungs of *Tlr4*$^{-/-}$ mice (Fig. 2K), demonstrating the role of TLR4 in promoting pulmonary edema. Moreover, as shown by the Kaplan-Meier survival curves, *Tlr4*$^{-/-}$ mice exhibited significantly improved survival outcomes after CLP. Over a 96-hour period post-CLP, *Tlr4*$^{-/-}$ mice demonstrated a pronounced survival advantage over the WT mice (Fig. 2L).

In summary, these findings demonstrate that TLR4 plays a pivotal role in the progression of sepsis-induced ALI, and its absence can lead to reduced lung injury, decreased inflammation, enhanced vascular integrity, and improved survival outcomes.

TLR4 deficiency alters cellular composition and attenuates inflammatory pathway activation in the septic lung

We employed Milo analysis to assess differential abundance among lung cell types across experimental groups. Milo assigns cells to overlapping neighborhoods on a k-nearest neighbor (KNN) graph, allowing the detection of continuous changes in cell states and trajectories[21]. In the WT CLP group, we identified significant increases in the abundance of SMC (median $\log_2$ fold change: +3.43), myeloid cell (median $\log_2$ fold change: +3.36), and fibroblast (median $\log_2$ fold change: +1.85), relative to the WT Sham group. In contrast, the abundance of EC was significantly reduced (median $\log_2$ fold change: -7.08), indicating a substantial shift in cellular composition in the WT CLP group (Fig. 3A and Supplementary Fig. 3A).

When comparing the WT CLP group to the *Tlr4*$^{-/-}$ CLP group, Milo analysis revealed an increased abundance of SMC (median $\log_2$ fold change: +2.20) and fibroblast (median $\log_2$ fold change: +2.35) in the WT CLP group. Conversely, there was a marked reduction in the abundance of myeloid cells (median $\log_2$ fold change: -2.46), epithelial cell (median $\log_2$ fold change: -2.49), and EC (median $\log_2$ fold change: -5.98) in the WT CLP group compared to the *Tlr4*$^{-/-}$ CLP group, highlighting the effect of TLR4 on these cell populations (Fig. 3B and Supplementary Fig. 3B).

Subsequently, we used AUCell to assess pathway activity at the single-cell level. We focused on the HALLMARK_INFLAMMATORY_RESPONSE and GOBP_POSITIVE_REGULATION_OF_REACTIVE_OXYGEN_SPECIES_BIOSYNTHETIC_PROCESS gene sets from MSigDB. The WT CLP group consistently showed the highest AUC scores for both the inflammatory response and ROS-related gene sets, indicating elevated pathway activity compared to other groups. This heightened activity aligns with the increased recruitment and activation of immune cells observed in prior analyses. Among all cell types, myeloid cells displayed the highest AUC scores, suggesting that

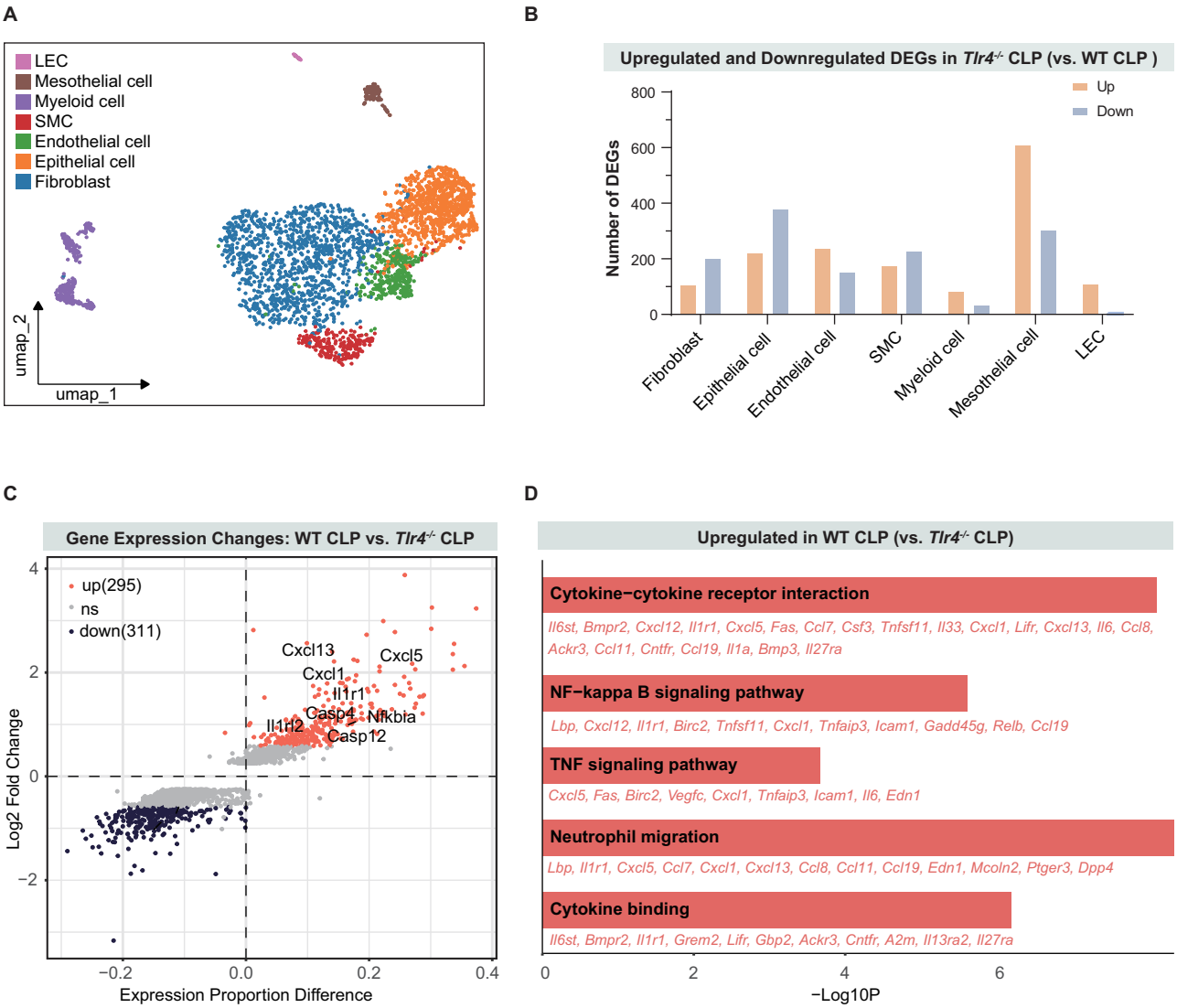

Fig. 1 | Genetic deletion of TLR4 exhibits wide transcriptomic alterations in the lungs following sepsis. A UMAP visualization of a total of 18,152 cells from all 14 lungs sample (WT Sham n = 3, *Tlr4*$^{-/-}$ Sham n = 4, WT CLP 24 h n = 4, and *Tlr4*$^{-/-}$ CLP 24 h n = 3), clustered into 7 cell types based on relative markers. **B** The number of upregulated and downregulated DEGs across specific cell types in the WT CLP group compared to the *Tlr4*$^{-/-}$ CLP group. **C** The gene expression changes between the *Tlr4*$^{-/-}$ CLP and WT CLP groups. The x-axis represents the difference in expression proportion and the y-axis shows the $\log_2$ fold change. **D** The pathways that are upregulated in the WT CLP group compared to the *Tlr4*$^{-/-}$ CLP group. The x-axis represents the negative logarithm of the *p*-value (-Log10P), which indicates the statistical significance of the upregulation. Each bar shows the extent of pathway enrichment, with longer bars indicating stronger significance. Specific genes involved in each pathway are listed next to the pathway name.

they are the primary drivers of inflammatory and oxidative stress responses in the lungs following CLP-induced sepsis (Fig. 3C–F and Supplementary Fig. 3C, D).

TLR4 deficiency reprograms macrophage polarization from pro-inflammatory to anti-inflammatory phenotype during sepsis

To investigate the myeloid cell heterogeneity in sepsis-induced ALI, we performed an unbiased clustering analysis of myeloid cells using scRNA-seq. The analysis revealed distinct myeloid cell populations, predominantly comprised of two major macrophage subsets, designated as macrophage_C1 and macrophage_C2, alongside the neutrophil population (Fig. 4A and Supplementary Fig. 3E). Quantitative analysis demonstrated that macrophages constituted the vast majority of myeloid cells, with macrophage_C1 representing 55.9% and macrophage_C2 accounting for 34.0% of the total myeloid cell population. In contrast, neutrophils comprised a relatively small fraction (10.1%) of the analyzed cells (Fig. 4B). Given the limited representation of neutrophils in the dataset, we focused our subsequent analyses on characterizing the predominant macrophage populations.

Initial transcriptional profiling revealed distinct molecular signatures between the macrophage subsets. Macrophage_C1 was characterized by elevated expression of genes associated with tissue repair and immunomodulation (e.g., *Pf4*, *Stab1*, *C1qa*, *Arg1*, *Spp1*, and *Ms4a4a*), while macrophage_C2 exhibited enrichment of genes involved in inflammatory responses (e.g., *Pparg*, *Il18*, *Chil3*, *Sort1*, *Mcemp1*, and *Ms4a8a*) (Fig. 4C). Although these gene signatures partially overlapped with classical M1/M2 markers, the transcriptional profiles revealed complex phenotypes that extend beyond the traditional M1/M2 dichotomy, reflecting the dynamic and heterogeneous nature of macrophage activation in sepsis-induced ALI. Further investigation of these macrophage subsets across experimental groups revealed a critical role for TLR4 signaling in regulating their distribution. In WT CLP, macrophage_C1 comprised 52.8% of macrophages, while macrophage_C2 accounted for 47.2%. Notably, TLR4 deficiency significantly altered this distribution, with macrophage_C1 markedly increasing to 68.7% and macrophage_C2 decreasing to 31.3% (Fig. 4D). Those shift in macrophage populations suggests that TLR4 signaling plays a crucial role in regulating macrophage phenotype and function during sepsis-induced ALI.

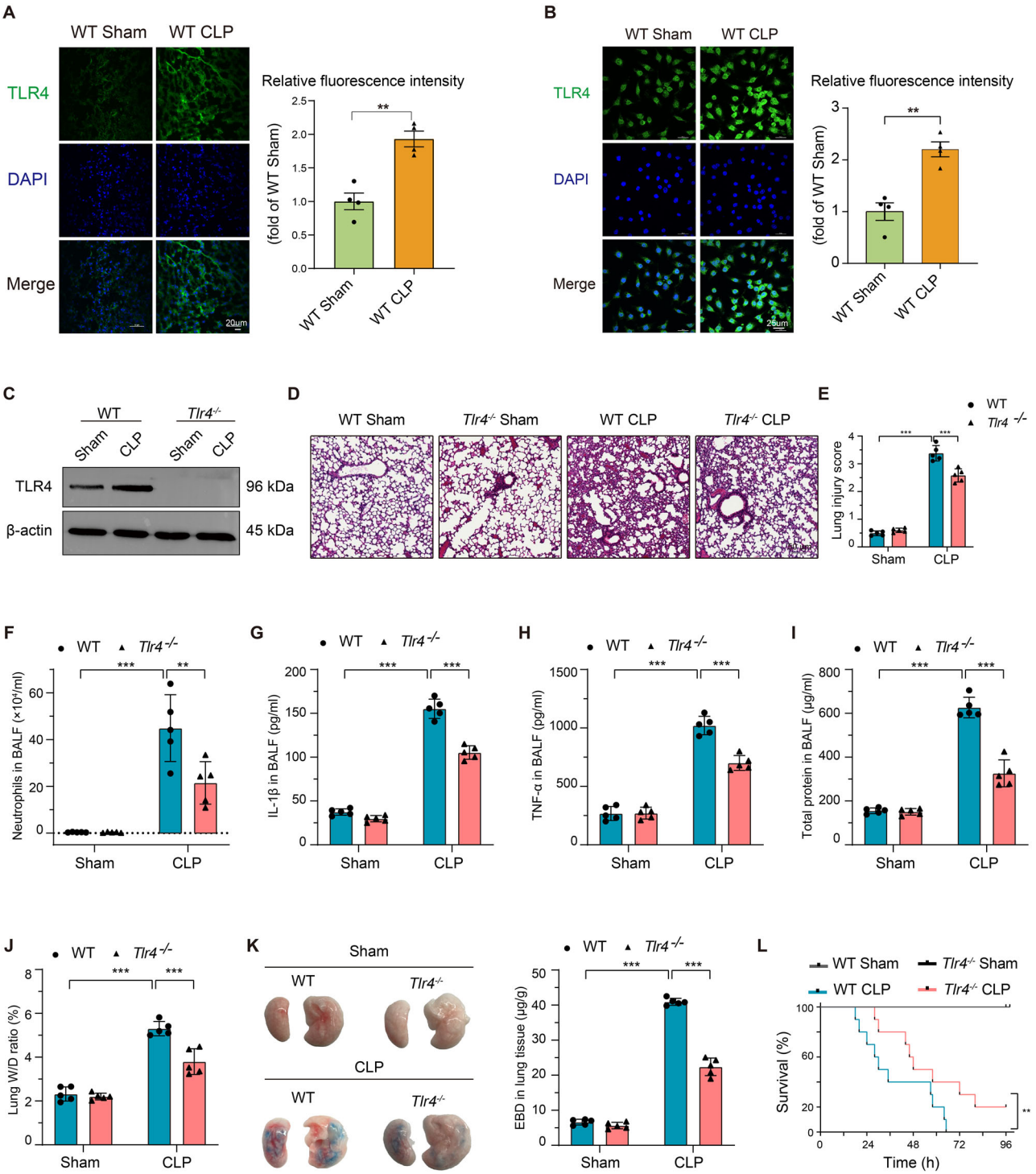

Fig. 2 | The phenotypic changes in sepsis-induced lung injury are consistent with the transcriptomic alterations caused by TLR4 deficiency. A Immunofluorescence detection of TLR4 expression in lung tissue 24 h post-CLP, with quantification of relative fluorescence intensity of TLR4 normalized to WT Sham, expressed as fold change (n = 4). Scale bar, 20 μm. **B** Immunofluorescence detection and quantification of TLR4 expression in macrophages from BALF of mice (n = 4). Scale bar, 25 μm. **C** Western blot analysis for TLR4 in lung tissues of WT and *Tlr4*$^{-/-}$ mice at 24 h post-CLP and sham procedures. **D** H&E staining of lung sections from WT and *Tlr4*$^{-/-}$ mice 24 h post-sham or CLP. Scale bar, 50 μm. **E** Lung injury scores were obtained from the pathological assessment of lung tissues (n = 5). **F** Quantification of neutrophilic granulocytes in the BALF (n = 5). **G**, **H** Levels of pro-inflammatory cytokines IL-1β and TNF-α in BALF were quantified using ELISA (n = 5). **I** Protein levels in BALF, indicative of vascular permeability, were assessed using BCA assay (n = 5). **J** Lung wet/dry weight ratio in WT and *Tlr4*$^{-/-}$ mice, indicative of pulmonary edema, after CLP (n = 5). **K** Lung damage and vascular permeability were assessed using the EBD extravasation method, with quantification of extracted EBD from lung tissue performed via spectrophotometry (n = 5). **L** Kaplan-Meier survival curves illustrate the survival probability of WT and *Tlr4*$^{-/-}$ mice subjected to sham or CLP over 96 h (n = 10). Data are represented as mean ± SD, $^{**}P < 0.01$, $^{***}P < 0.001$.

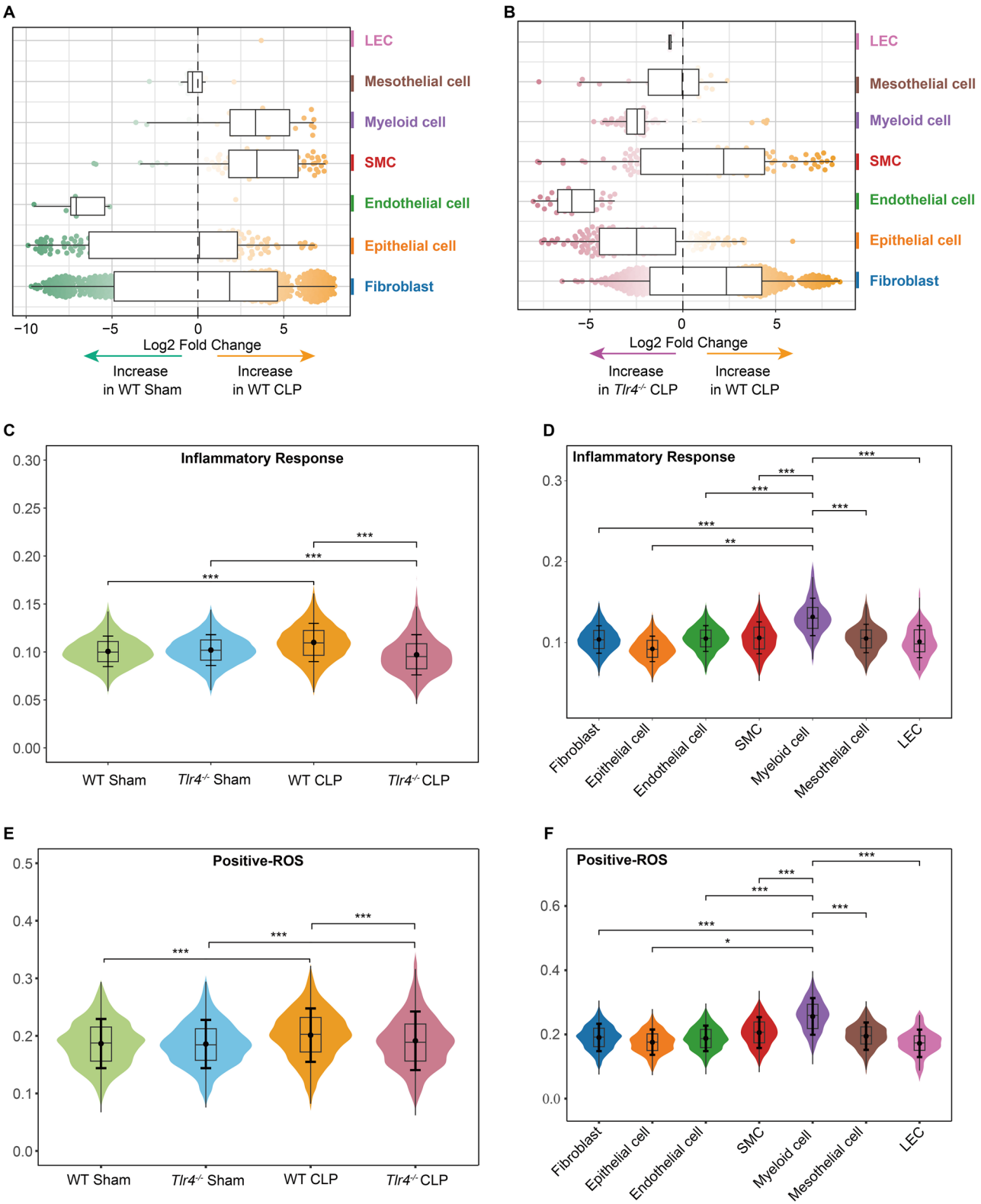

Fig. 3 | TLR4 deficiency alters cellular composition and attenuates inflammatory pathway activation in the septic lung. A The differential abundance analysis between WT Sham and WT CLP groups using Milo, a sophisticated statistical framework that detects compositional changes by analyzing partially overlapping cell neighborhoods constructed on a KNN graph. **B** The differential abundance analysis between the *Tlr4*$^{-/-}$ CLP and WT CLP groups. **C** The distribution of inflammatory response signatures across four groups: WT Sham, *Tlr4*$^{-/-}$ Sham, WT CLP, and *Tlr4*$^{-/-}$ CLP. The y-axis shows AUC scores from AUCell representing the inflammatory response signature. **D** The inflammatory response signatures across various cell types. **E** The distribution of positive ROS signatures across four groups. **F** The positive ROS signatures across various cell types. Data are presented as the median (interquartile range), $^{*}P < 0.05$, $^{**}P < 0.01$, $^{***}P < 0.001$.

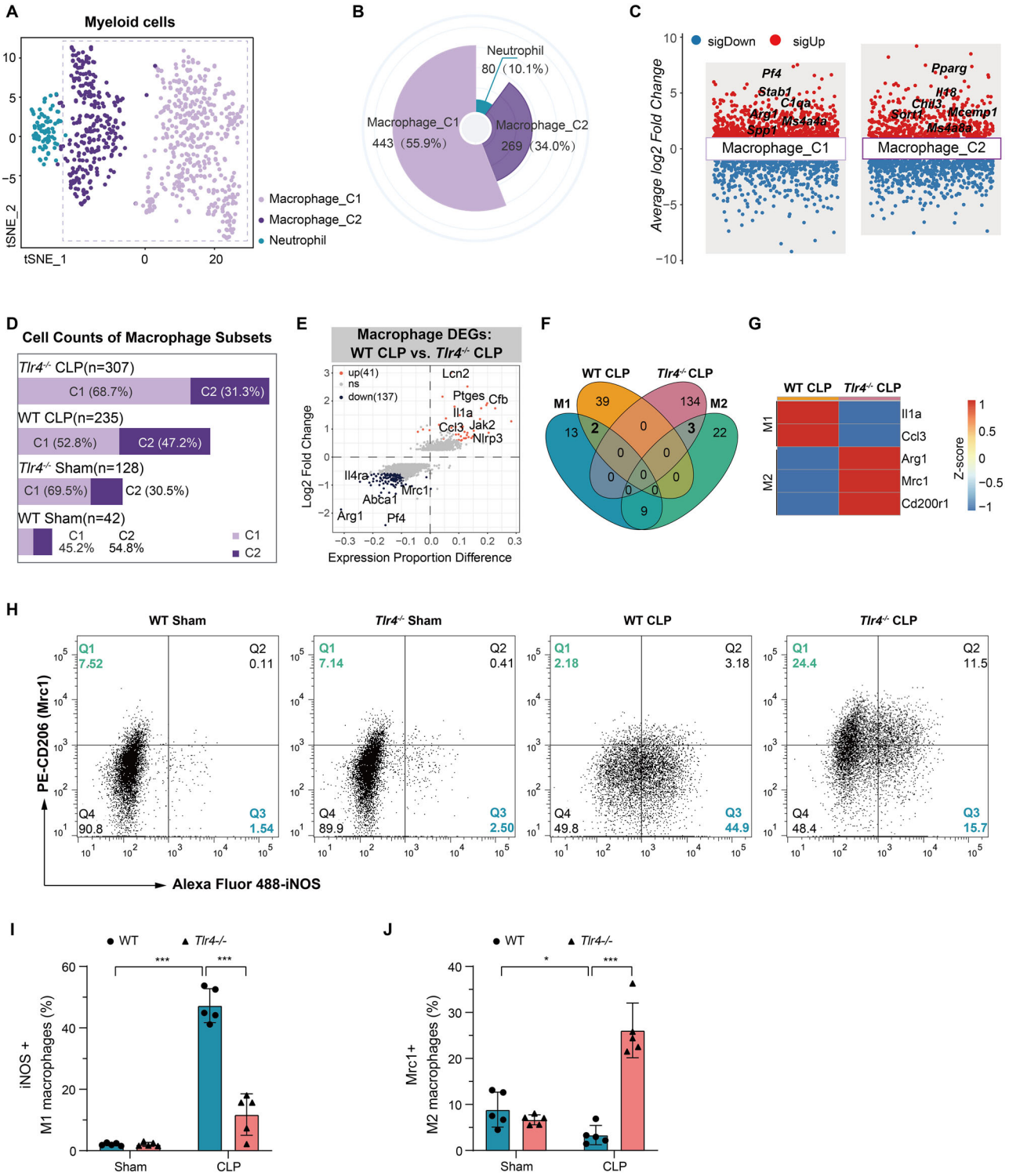

Fig. 4 | TLR4 deficiency reprograms macrophage polarization from pro-inflammatory to anti-inflammatory phenotype during sepsis. A t-SNE plot showing clustering of myeloid cells into two macrophage subsets (macrophage_C1 and macrophage_C2) and neutrophils. **B** Quantification of myeloid cells composition. **C** Differential expression analysis of macrophage_C1 and macrophage_C2. **D** Distribution of macrophage_C1 and macrophage_C2 across experimental groups. **E** Scatter plot illustrating macrophage gene expression changes between the WT CLP and *Tlr4*$^{-/-}$ CLP groups. **F** Venn diagram showing the overlap between upregulated genes in WT CLP and *Tlr4*$^{-/-}$ CLP groups, compared to known M1 and M2 macrophage markers (sourced from OriGene's M1 and M2 Macrophage Markers). The diagram illustrates the number of genes upregulated in each group, with the intersection highlighting genes shared across conditions. **G** Heatmap comparing the expression of key M1 markers (*Il1a* and *Ccl3*) and M2 markers (*Arg1*, *Mrc1*, and *Cd200r1*) between the WT CLP and *Tlr4*$^{-/-}$ CLP groups. The Z-score of expression is plotted, with red indicating higher expression and blue indicating lower expression. WT CLP shows higher expression of M1 markers, while *Tlr4*$^{-/-}$ CLP shows elevated expression of M2 markers. **H** Flow cytometry of macrophages isolated from BALF, showing percentages of iNOS^{+} and Mrc1^{+} macrophages across experimental groups. **I, J** Quantitative analysis of M1 and M2 macrophage proportions (n = 5). Data are represented as mean ± SD, $^{*}P < 0.05$, $^{***}P < 0.001$.

We next performed comprehensive gene expression analysis to compare macrophage phenotypes between WT CLP and *Tlr4*$^{-/-}$ CLP groups. Differential gene expression analysis revealed distinct transcriptional signatures: WT CLP macrophages showed marked upregulation of pro-inflammatory genes, including *Lcn2*, *Ptges*, *Cfb*, *Nlrp3*, *Il1a*, and *Ccl3*, whereas *Tlr4*$^{-/-}$ CLP macrophages predominantly expressed anti-inflammatory genes such as *Il4ra*, *Mrc1*, and *Arg1* (Fig. 4E). Venn diagram analysis was used to compare upregulated genes in each group with known M1 (pro-inflammatory) and M2 (anti-inflammatory) macrophage markers (Fig. 4F). WT CLP macrophages prominently expressed M1 genes *Il1a* and *Ccl3*, whereas *Tlr4*$^{-/-}$ CLP macrophages showed elevated levels of M2 markers *Mrc1*, *Arg1*, and *Cd200r1* (Fig. 4F, G).

To validate these transcriptional findings at the protein level, we performed flow cytometric analysis of macrophages isolated from BALF. Consistent with the gene expression data, the WT CLP group had significantly more iNOS^{+} (M1) macrophages, indicating enhanced pro-inflammatory activation. In contrast, the *Tlr4*$^{-/-}$ CLP group exhibited a higher proportion of Arg1^{+} and Mrc1^{+} (M2) macrophages, suggesting a shift toward an anti-inflammatory phenotype in the absence of TLR4 (Fig. 4H–J and Supplementary Fig. 4C, D).

TLR4 ablation promotes metabolic reprogramming and mitochondrial homeostasis in septic macrophages

Following the analysis of macrophage polarization, we further explored how metabolic reprogramming contributes to the functional differences between WT CLP and *Tlr4*$^{-/-}$ CLP macrophages. Cellular metabolic changes, particularly in glycolysis and oxidative phosphorylation (OXPHOS), are critical for determining macrophage polarization and function[22,23]. M1 macrophages typically exhibit increased glycolytic activity [24], while M2 macrophages rely more on oxidative metabolism[25]. To assess these metabolic shifts, we quantified glycolysis, OXPHOS, and ROS activity in macrophages across the four experimental groups. Our analysis revealed significant metabolic reprogramming in response to TLR4 signaling during sepsis, particularly favoring glycolysis and ROS production in the WT CLP group, while *Tlr4*$^{-/-}$ CLP mice maintained higher OXPHOS activity, indicating a shift away from glycolytic metabolism (Fig. 5A).

This metabolic divergence was further supported by elevated lactate levels in the WT CLP group, consistent with increased glycolytic flux, while the *Tlr4*$^{-/-}$ CLP group showed reduced glucose consumption, as confirmed by FITC-2-NBDG uptake (Fig. 5B, C). In contrast, *Tlr4*$^{-/-}$ CLP mice maintained lower NADH levels and a more favorable NAD^{+}/NADH ratio, reflecting preserved oxidative metabolism and mitochondrial function (Fig. 5D, E). Additionally, adenosine triphosphate (ATP) levels were better sustained in the *Tlr4*$^{-/-}$ CLP group, indicating a more balanced energy metabolism through OXPHOS (Fig. 5F).

Moreover, ROS production was markedly higher in the WT CLP group, signifying enhanced oxidative stress under TLR4-mediated inflammation, whereas the *Tlr4*$^{-/-}$ CLP group displayed significantly lower ROS levels (Fig. 5G). Finally, JC-1 staining demonstrated that mitochondrial integrity was compromised in the WT CLP group, while *Tlr4*$^{-/-}$ CLP mice maintained healthier mitochondrial function (Fig. 5H).

These findings collectively demonstrate that TLR4 modulates macrophage metabolic reprogramming by promoting glycolysis and ROS production, while *Tlr4*$^{-/-}$ CLP mice maintain mitochondrial integrity and shift towards OXPHOS, suggesting a protective metabolic adaptation in the absence of TLR4.

TLR4 deficiency alleviates cholesterol efflux suppression in septic macrophages

Given that ATP-binding cassette transporter A1 (ABCA1) is a key regulator of cholesterol efflux[26], we further investigated the role of TLR4 in modulating lipid metabolism and cholesterol efflux in macrophages. Gene expression analysis between the WT CLP and *Tlr4*$^{-/-}$ CLP macrophage groups revealed a significant upregulation of *Abca1* in the *Tlr4*$^{-/-}$ CLP group (Fig. 4E). The AUC scores derived from scRNA-seq analysis indicated that the *Tlr4*$^{-/-}$ CLP group exhibited enhanced lipid metabolism and cholesterol efflux activity compared to the WT CLP group (Fig. 6A), aligning with the upregulation of *Abca1* observed in the *Tlr4*$^{-/-}$ CLP group (Figs. 4E and 6B). Immunofluorescence staining of lung tissues further supported these findings, showing an increased number of F4/80^{+} ABCA1^{+} macrophages in the *Tlr4*$^{-/-}$ CLP group, indicating higher ABCA1 expression in the absence of TLR4 (Fig. 6C). Additionally, ABCA1 expression in macrophages isolated from BALF was significantly elevated in the *Tlr4*$^{-/-}$ CLP group compared to the WT CLP group (Fig. 6D).

The functional activity of cholesterol efflux was assessed in vitro by incubating macrophages with a cholesterol acceptor (serum) for 6 h, revealing that *Tlr4*$^{-/-}$ CLP macrophages exhibited significantly higher cholesterol efflux compared to WT CLP macrophages (Fig. 6E), suggesting that TLR4 deficiency alleviates the suppression of cholesterol efflux observed during sepsis. Importantly, previous studies have shown that impaired cholesterol efflux is associated with exacerbated inflammation[27,28], suggesting that disrupted lipid metabolism may contribute to a heightened inflammatory response in various diseases, including sepsis[29]. Therefore, the increased cholesterol efflux observed in the *Tlr4*$^{-/-}$ CLP group may help mitigate inflammation by alleviating lipid accumulation and cellular stress. Subsequently, we measured the levels of pro-inflammatory cytokines in macrophage supernatants after 6 h of in vitro culture without any additional treatment. WT CLP macrophages secreted significantly higher levels of IL-1α, IL-1β, IL-6, and TNF-α compared to *Tlr4*$^{-/-}$ CLP macrophages (Fig. 6F–I).

In summary, these findings demonstrate that TLR4 plays a pivotal role in coordinating macrophage metabolic reprogramming, regulating cholesterol efflux, and driving inflammatory cytokine production. *Tlr4*$^{-/-}$ CLP macrophages exhibit a more anti-inflammatory and metabolically adaptive phenotype during sepsis-induced ALI, highlighting the protective effects of TLR4 deficiency in modulating these processes.

Loss of TLR4 modifies the cellular cross-talk between macrophages and pulmonary ECs/LECs

To explore the impact of TLR4 on macrophage-EC and macrophage-LEC interactions during sepsis-induced ALI, we utilized CellChat analysis based on scRNA-seq data (Fig. 7A). This analysis identified pivotal ligand-receptor (L-R) pairs mediating crosstalk between macrophages and both ECs and LECs. CellChat detected 66 L-R pairs involving macrophage-derived ligands and EC/LEC receptors, displaying varying interaction probabilities under different conditions (Fig. 7B, C).

In examining macrophage-EC (Mϕ → EC) interactions, distinct differences between the WT CLP and *Tlr4*$^{-/-}$ CLP groups were found. Specific L-R pairs such as *Tgfb1-(Acvr1+Tgfbr1)*, *Tgfb1-(Tgfbr1+Tgfbr2)*, *Lgals9-Cd44/P4hb*, and *Col1a1/Col1a2/Col4a1-(Itga2+Itgb1)* were significantly elevated in the *Tlr4*$^{-/-}$ CLP group compared to WT CLP (Fig. 7B). Notably, TGF-β (encoded by *Tgfb1*) is well-documented for its role in promoting vascular homeostasis and facilitating endothelial repair[30], LGALS9 (encoded by *Lgals9*), through its interactions with receptors like CD44, has been associated with tissue remodeling and anti-inflammatory effects, supporting cellular repair processes[31]. In contrast, the WT CLP group exhibited elevated pro-inflammatory interactions such as *Il1a-(Il1r1+Il1rap)* and *Spp1-(Itga8+Itgb1)*, particularly the Il1a-IL1 receptor pathway, which is crucial for sustaining inflammatory responses in sepsis[32,33] (Fig. 7B).

For the macrophage-LEC (Mϕ → LEC) interactions, we also observed significant changes between the WT CLP and *Tlr4*$^{-/-}$ CLP groups. The WT CLP group exhibited increased pro-inflammatory L-R pairs, including *Il1a-(Il1r1+Il1rap)*, *Cxcl12-Cxcr4*, *Thbs1-Cd36*, and *(Itgav+Itgb1)-Adgre5* (Fig. 7C), which are known to promote inflammatory signaling and leukocyte adhesion. Conversely, the *Tlr4*$^{-/-}$ CLP group showed heightened engagement in L-R pairs linked to tissue repair and anti-inflammatory functions, including *Lgals9-P4hb*, *Ccl4-Ackr2*, *Ccl3-Ackr2*, and *Ccl2-Ackr2*. Additionally, signaling associated with vascular development and ECM stability—such as *Vegfd-Vegfr3*, *Vegfd-Vegfr2r3*, *Tgfb1-(Tgfbr1+Tgfbr2)*, and *Selplg-Selp*—was more prominent in the *Tlr4*$^{-/-}$ CLP group (Fig. 7C).

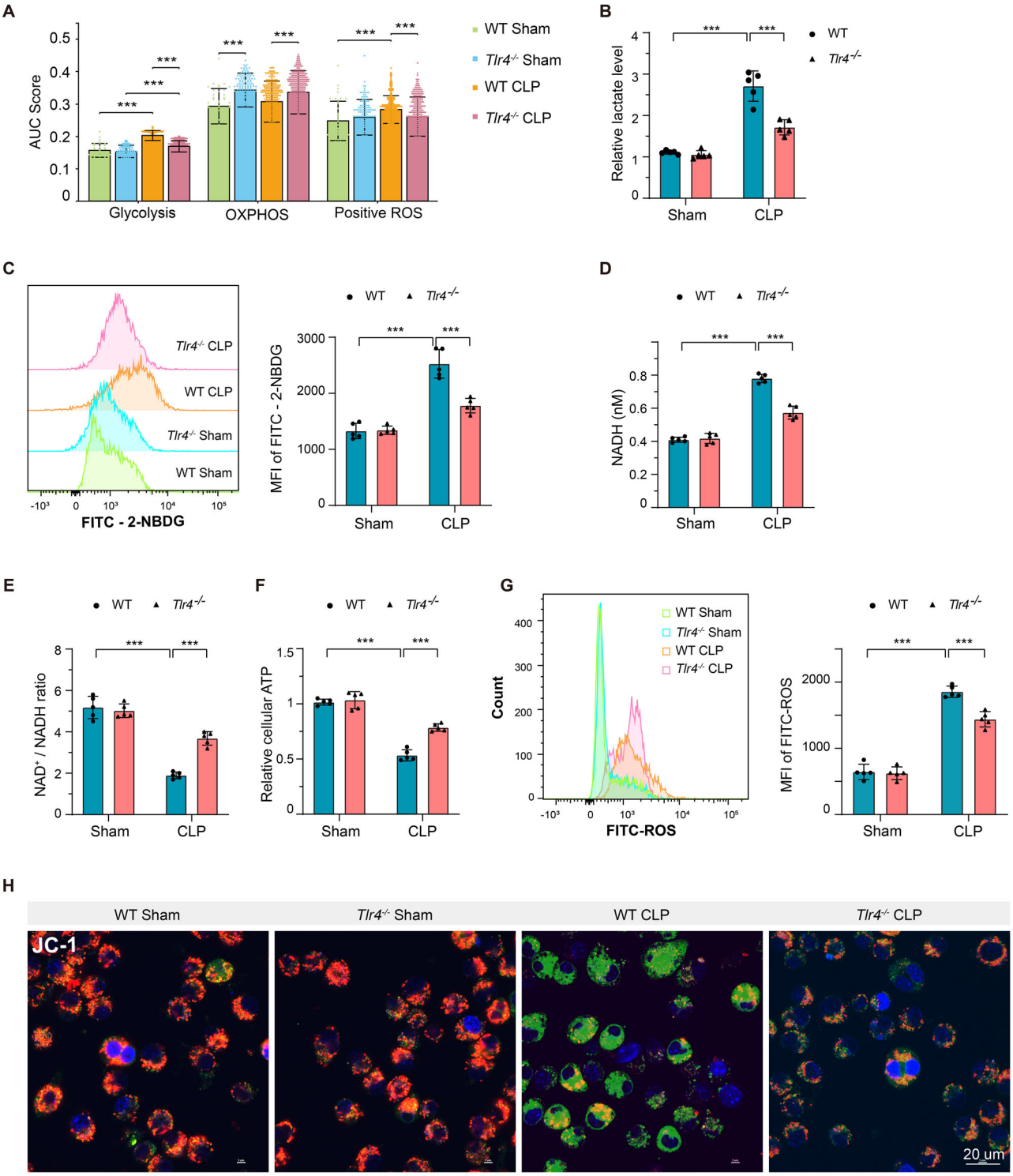

Fig. 5 | TLR4 ablation promotes metabolic reprogramming and mitochondrial homeostasis in septic macrophages. A The AUC scores for glycolysis, OXPHOS, and positive ROS from scRNA-seq analysis across the four groups. Increased glycolysis and ROS production were observed in the WT CLP group, while the *Tlr4*$^{-/-}$ CLP group showed higher OXPHOS activity compared to WT CLP. **B** The relative lactate levels in macrophages from the BALF of each mouse group (n = 5). **C** Flow cytometry quantifying glucose uptake (FITC-2-NBDG) across the four groups (n = 5). **D** The NADH levels in macrophages from the BALF of each mouse group (n = 5). **E** Bar graph illustrating the NAD^+ / NADH ratio, indicating a shift towards glycolysis in the WT CLP group (n = 5). **F** Relative amounts of intracellular ATP in WT and *Tlr4*$^{-/-}$ macrophages (n = 5). **G** Levels of ROS were measured in macrophages from the BALF via flow cytometry (n = 5). **H** JC-1 staining of mitochondrial membrane potential in macrophages from each group. The WT CLP group shows greater mitochondrial dysfunction (green staining) compared to the other groups, with *Tlr4*$^{-/-}$ CLP showing more preserved membrane potential. Data are represented as mean ± SD, $^{***}P < 0.001$.

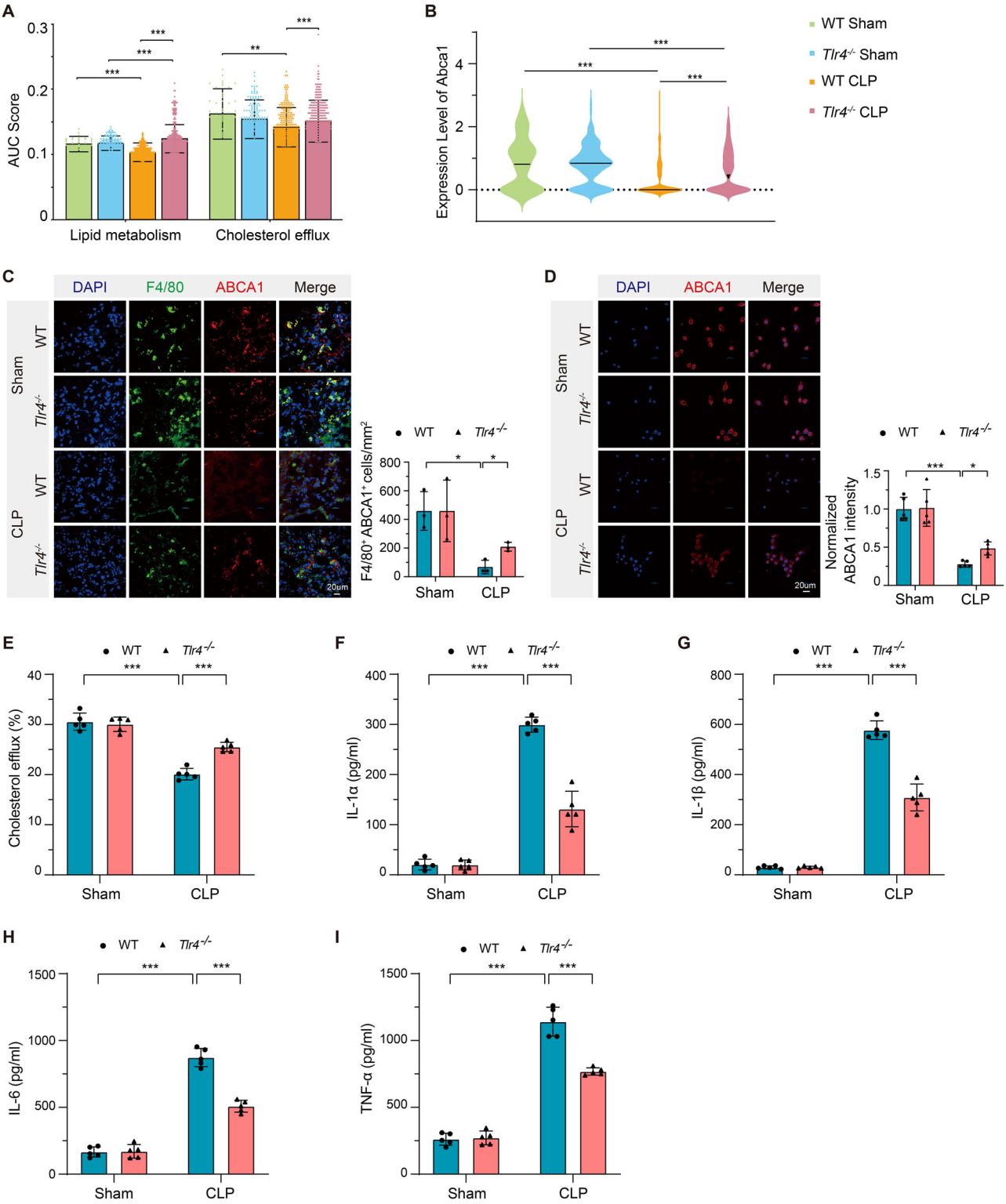

Fig. 6 | TLR4 deficiency alleviates cholesterol efflux suppression in septic macrophages. A The AUC scores for lipid metabolism and cholesterol efflux from scRNA-seq analysis across the four groups. **B** The expression level of Abca1 from scRNA-seq analysis across the four groups. **C** Representative immunofluorescence images of lung tissue stained with F4/80 (green) and ABCA1 (red) in the four groups. The bar graph quantifies the number of F4/80$^+$ ABCA1$^+$ macrophages per mm^2 (n = 3). Scale bar, 20 μm. **D** Immunofluorescence detection and quantification of ABCA1 expression in macrophages from BALF of mice (n = 5). Scale bar, 20 μm. **E** Bar graph showing cholesterol efflux (%) in macrophages isolated from BALF and incubated with a cholesterol acceptor (serum) for 6 hours in vitro. **F–I** Bar graphs showing concentrations of pro-inflammatory cytokines (IL-1α, IL-1β, IL-6, and TNF-α) in macrophage supernatants after 6 hours of in vitro culture without any additional treatment. Data are represented as mean ± SD or median (interquartile range), $^*P < 0.05$, $^{**}P < 0.01$, $^{***}P < 0.001$.

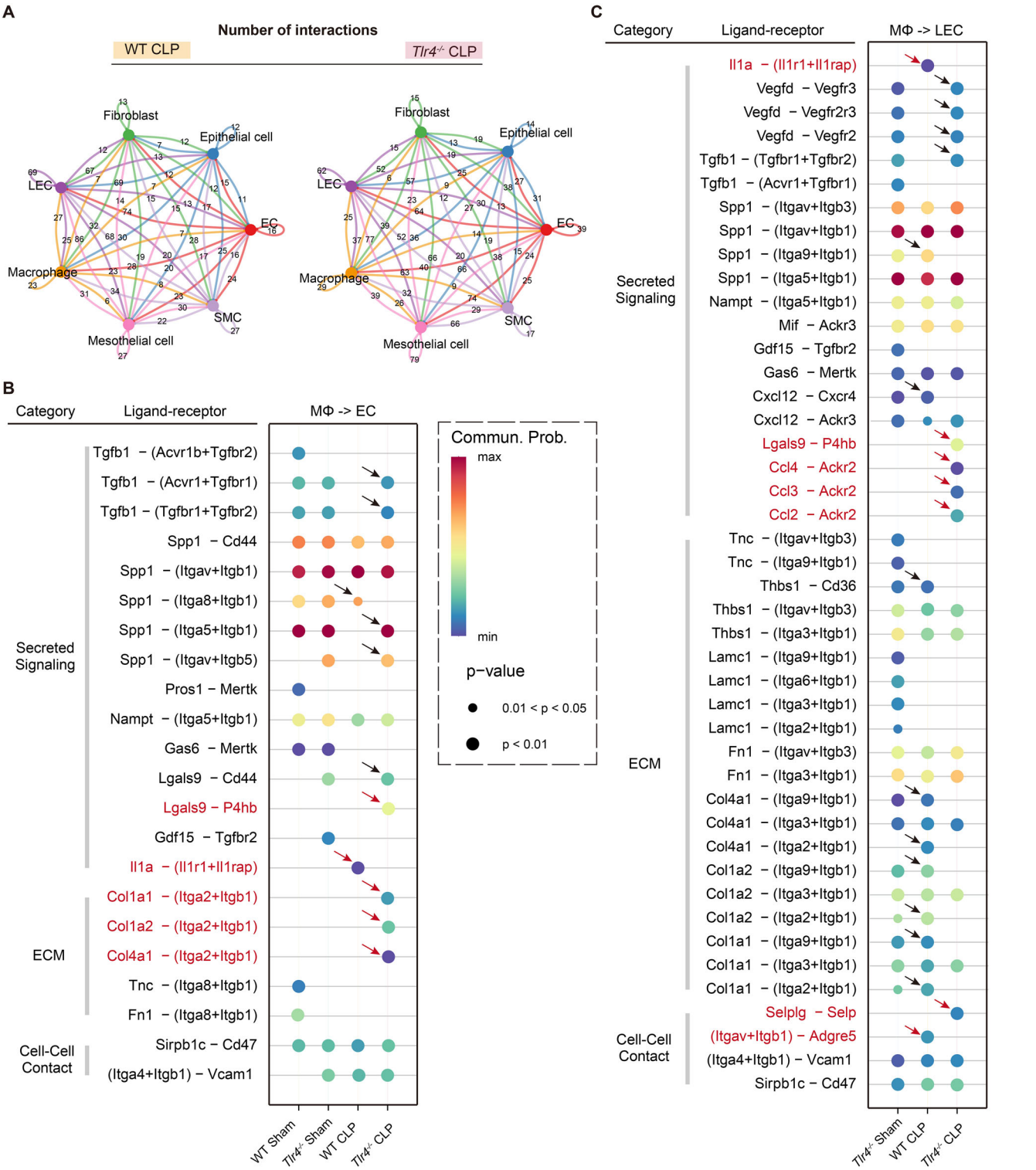

Fig. 7 | Loss of TLR4 modifies the cellular cross talk between macrophages and pulmonary ECs/LECs. A Network plots showing the number of L-R pairs involved in interactions between different lung cell types in the WT CLP and *Tlr4*$^{-/-}$ CLP groups. The numbers on each line represent the number of L-R pairs mediating interactions between the cell types. **B** Predicted L-R interactions that macrophages (Mϕ) exert on ECs across secreted signaling, extracellular matrix (ECM), and cell-cell contact categories, inferred by the CellChat R package. **C** Predicted L-R interactions that Mϕ exert on LECs. Dot size reflects *p*-value and color indicates communication probability. Arrows highlight key differences between the WT CLP and *Tlr4*$^{-/-}$ CLP groups.

Taken together, TLR4 deficiency shifts Mϕ-EC/LEC interactions towards pathways that support endothelial stability, reduce inflammation, and promote vascular integrity. This suggests that targeting TLR4 could be beneficial in managing sepsis-induced lung injury.

TLR4-deficient macrophages protect endothelial function and barrier integrity during sepsis

To investigate the role of TLR4 in macrophage-induced damage to pulmonary ECs and LECs during sepsis, macrophages were isolated from the

BALF of WT Sham, *Tlr4*$^{-/-}$ Sham, WT CLP, and *Tlr4*$^{-/-}$ CLP mice and co-cultured with WT pulmonary ECs and LECs in a Transwell system for 24 h (Fig. 8A). Mitochondrial status and oxidative stress in ECs and LECs were assessed by confocal microscopy with staining of JC-1 and FITC-ROS. Both ECs and LECs co-cultured with WT CLP macrophages exhibited significant mitochondrial depolarization, as evidenced by increased green fluorescence in JC-1 staining and elevated ROS levels. In contrast, *Tlr4*$^{-/-}$ CLP macrophages preserved mitochondrial membrane potential and reduced ROS levels in both ECs and LECs (Fig. 8B–E).

To quantify cell damage, Annexin V and PI staining were used to assess cell death patterns. Flow cytometry revealed a significant increase in late apoptotic/secondary necrotic (PI^+ Annexin V^+) ECs and LECs after co-culture with WT CLP macrophages, whereas *Tlr4*$^{-/-}$ CLP macrophages substantially reduced the proportion of PI^+ Annexin V^+ cells in both cell types (Fig. 8F). Endothelial integrity was further evaluated by analyzing the expression of tight junction proteins ZO-1 and Occludin. In WT ECs and LECs, co-culture with WT CLP macrophages significantly reduced ZO-1 and Occludin levels, indicating disrupted tight junctions. However, *Tlr4*$^{-/-}$ CLP macrophages preserved the expression of these proteins, maintaining the structural integrity of both ECs and LECs (Fig. 8G, H). To validate the findings' functional connections, we assessed endothelial barrier function using FITC-dextran permeability assays. Consistent with the observed cellular damage and disrupted tight junctions, ECs co-cultured with WT CLP macrophages exhibited a significant increase in permeability. In contrast, ECs exposed to *Tlr4*$^{-/-}$ CLP macrophages showed marked lower permeability, indicating better preservation of barrier function (Supplementary Fig. 4E).

Collectively, these findings demonstrate the critical role of TLR4 in mediating macrophage-induced endothelial damage during sepsis-induced ALI by impairing mitochondrial function, inducing oxidative stress and necrotic cell death, and damaging endothelial tight junction integrity.

Endothelial TLR4 mediates cell injury through both direct LPS sensing and macrophage-dependent pathways

To further determine whether the observed changes in pulmonary ECs and LECs function during sepsis (Fig. 2) are driven by TLR4 in ECs/LECs or indirectly through macrophage-derived signals, we investigated the role of TLR4 on ECs and LECs during sepsis. In the macrophage co-culture system, ECs and LECs were exposed to macrophages isolated from BALF of WT sham or CLP mice. WT ECs co-cultured with CLP-activated macrophages demonstrated significantly elevated ROS production compared to the group co-cultured with macrophages from sham animals, while *Tlr4*$^{-/-}$ ECs exhibited marked resistance to oxidative stress (Fig. 9A). Parallel findings were observed in LECs, where TLR4 deficiency similarly attenuated macrophage-induced ROS generation (Fig. 9B). Moreover, flow cytometric analysis revealed that genetic ablation of TLR4 in both ECs and LECs conferred protection against macrophage-induced proportion of late apoptotic/secondary necrotic cells (Fig. 9C), establishing TLR4 as a critical mediator of macrophage-endothelial inflammatory signaling.

To examine the direct effects of TLR4 activation, we challenged isolated ECs and LECs with LPS (10 μg/ml, 24 h). WT ECs/LECs exhibited pronounced increases in both ROS production (Fig. 9D, E) and progression to late apoptotic/secondary necrotic cell death (Fig. 9F) following LPS exposure. In contrast, *Tlr4*$^{-/-}$ cells demonstrated significant resistance to LPS-induced oxidative stress and necrotic cell death, indicating that endothelial TLR4 directly mediates LPS-induced cellular injury.

Collectively, these findings demonstrate that TLR4 promotes endothelial dysfunction through both indirect macrophage-mediated signaling and direct LPS-induced cellular responses.

Discussion

Over the past few decades, the roles of TLR4 in inflammation have been extensively studied. However, many details of the TLR4-related mechanisms remain poorly understood. Gaining new insights into the TLR4-regulated mechanism is still urgently needed. The current study addresses several previously unanswered questions. First, by employing scRNA-seq, the study offers the first comprehensive landscape of TLR4-dependent cellular and molecular changes in sepsis-induced ALI, revealing previously unrecognized, cell-type specific responses. Second, TLR4 drives macrophage polarization toward a pro-inflammatory phenotype while simultaneously modulating their metabolic state through enhanced glycolysis and suppressed OXPHOS. Third, TLR4 regulates macrophage cholesterol efflux through ABCA1, linking lipid metabolism to inflammatory responses. Finally, we identified a previously unrecognized mechanism through which TLR4 mediates endothelial damage by promoting macrophage-EC/LEC interactions and directly sensitizing ECs/LECs to both LPS stimulation and macrophage-derived inflammatory signals.

Cellular metabolism plays a crucial role in regulating macrophage function. Our single-cell transcriptomic analysis suggests that TLR4 deficiency significantly affects the metabolic profile of pulmonary macrophages, particularly in the regulation of glycolysis and OXPHOS. While septic WT macrophages showed enhanced glycolysis and suppressed OXPHOS, *Tlr4*$^{-/-}$ macrophages maintained a more balanced metabolic state, as evidenced by reduced lactate production, elevated ATP levels, and preserved mitochondrial function. This metabolic adaptation aligns with previous studies showing that LPS-TLR4 signaling typically drives rapid metabolic reprogramming toward glycolysis to support inflammatory responses[34,35]. In this study, the TLR4-dependent metabolic shift was accompanied by elevated ROS levels and mitochondrial dysfunction, reflecting the metabolic feature of pro-inflammatory M1 macrophages[36]. The preservation of mitochondrial function in *Tlr4*$^{-/-}$ macrophages, along with their shift toward an anti-inflammatory M2-like phenotype, highlights TLR4's involvement in coupling metabolic adaptation with inflammatory responses in septic macrophages.

Dysregulated lipid metabolism, particularly impaired cholesterol efflux, has emerged as a critical link between metabolic dysfunction and inflammatory responses in sepsis-related organ dysfunction[29,37]. Cholesterol efflux, primarily mediated by ABCA1 and ATP-binding cassette transporters G1 (ABCG1), plays an essential role in maintaining cellular cholesterol homeostasis[26]. During sepsis, we observed significant suppression of ABCA1 expression in macrophages, which was partially reversed by TLR4 deficiency. This preservation of ABCA1 expression is crucial as it mediates cholesterol efflux from lipid rafts, specialized membrane microdomains that serve as platforms for inflammatory signaling[38,39]. Previous studies have shown that enhanced ABCA1-mediated cholesterol efflux from lipid rafts can attenuate inflammatory responses[29,40]. Notably, our functional studies revealed enhanced cholesterol efflux capacity and reduced inflammatory cytokine production (IL-1α, IL-1β, IL-6, and TNF-α) in *Tlr4*$^{-/-}$ macrophages during sepsis, suggesting a mechanistic link between TLR4-regulated cholesterol efflux and inflammatory responses.

Sepsis-induced ALI involves complex mechanisms that include cellular and molecular interactions between immune and lung parenchymal cells. Through CellChat analysis of single-cell transcriptomics data, we uncovered distinct communication patterns between macrophages and ECs/LECs during sepsis. Notably, *Tlr4*$^{-/-}$ macrophages exhibited enhanced expression of vascular protective factors (*Tgfb1* and *Lgals9*)[30,31] while showing reduced pro-inflammatory signaling (*Il1a*) compared to WT macrophages, suggesting a shift from inflammatory to reparative phenotype. Supporting these molecular signatures, functional co-culture experiments demonstrated that *Tlr4*$^{-/-}$ macrophages preserved endothelial barrier integrity and reduced oxidative stress-induced secondary necrotic cell death in both ECs and LECs.

Endothelial injury and dysfunction were markedly attenuated in *Tlr4*$^{-/-}$ mice, underscoring TLR4's crucial role in sepsis-induced pulmonary leakage. First, macrophage TLR4 mediates the production of inflammatory signals that induce endothelial injury, as evidenced by the protective effects of TLR4-deficient macrophages on barrier integrity of ECs and LECs. Second, endothelial TLR4 functions as a critical sensor determining cellular susceptibility to macrophage-derived inflammatory mediators, demonstrated by the enhanced resistance of TLR4-deficient ECs and LECs to

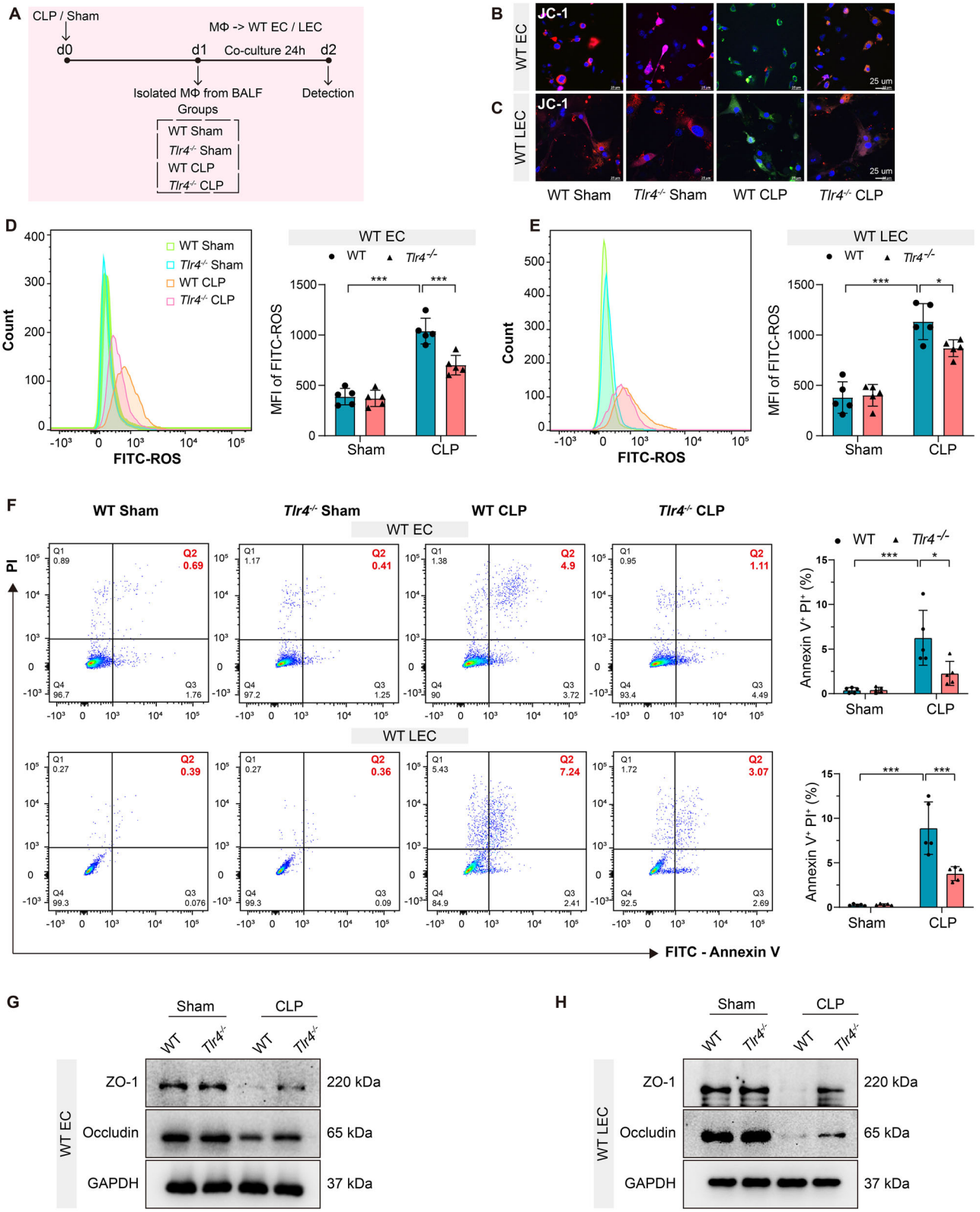

Fig. 8 | TLR4-deficient macrophages protect endothelial function and barrier integrity during sepsis. A Experimental setup: Mϕ isolated from the BALF of WT Sham, *Tlr4*$^{-/-}$ Sham, WT CLP, and *Tlr4*$^{-/-}$ CLP mice were co-cultured with ECs or LECs, isolated from the lung of WT mice, for 24 hours in a Transwell system. **B** Representative images of JC-1 staining in ECs after co-culture. Scale bar, 25 μm. **C** Representative images of JC-1 staining in LECs after co-culture. Scale bar, 25 μm. **D** Histogram and MFI analysis of ROS production in ECs. **E** Histogram and MFI analysis of ROS production in LECs. **F** Flow cytometry analysis of apoptosis using PI and Annexin V staining in ECs (top panel) and LECs (bottom panel). **G** Western blot analysis of ZO-1 and Occludin in ECs, with GAPDH as a loading control. **H** Western blot analysis of ZO-1 and Occludin in LECs. Data are represented as mean ± SD, $^{*}P < 0.05$, $^{***}P < 0.001$.

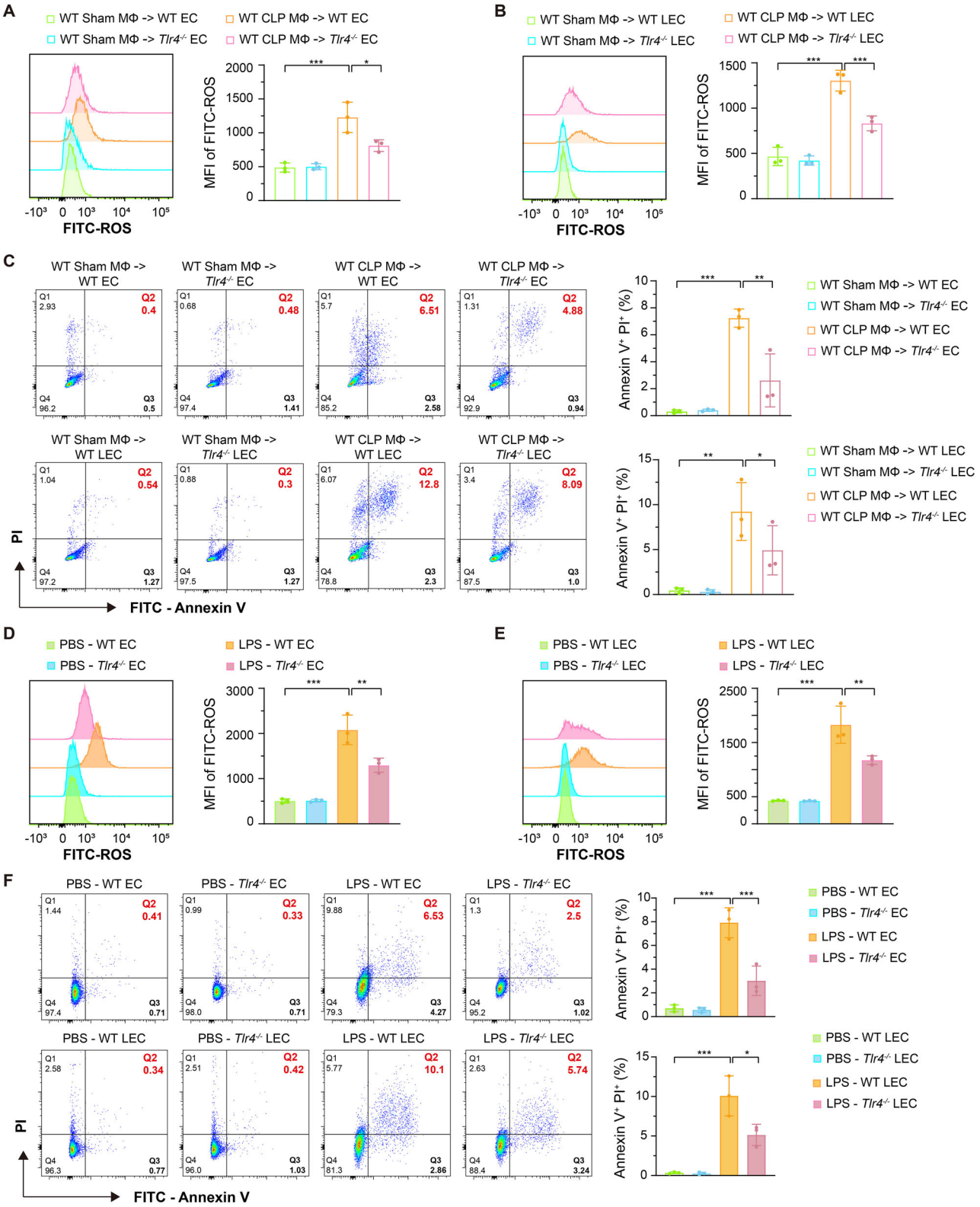

Fig. 9 | Endothelial TLR4 mediates cell injury through both direct LPS sensing and macrophage-dependent pathways. A ROS levels in WT or *Tlr4*$^{-/-}$ ECs following 24-hour co-culture with Mϕ isolated from BALF of WT Sham or WT CLP 24 h mice. **B** ROS levels in WT or *Tlr4*$^{-/-}$ LECs following 24-hour co-culture with Mϕ isolated from BALF of WT Sham or WT CLP 24 h mice. **C** Flow cytometry analysis of apoptosis in ECs (top panel) and LECs (bottom panel) following 24-hour co-culture with Mϕ. **D** ROS levels in WT or *Tlr4*$^{-/-}$ ECs after 24-hour stimulation with 10 μg/ml LPS or an equivalent volume of PBS. **E** ROS levels in WT or *Tlr4*$^{-/-}$ LECs after 24-hour stimulation with 10 μg/ml LPS or an equivalent volume of PBS. **F** Flow cytometry analysis of apoptosis in ECs (top panel) and LECs (bottom panel) following 24-hour stimulation with 10 μg/ml LPS. Data are represented as mean ± SD, $^{*}P < 0.05$, $^{**}P < 0.01$, $^{***}P < 0.001$.

macrophage-induced stress and apoptosis. Supporting this finding, our previous work established that endothelial TLR4 mediates the endocytosis of DAMPs during sepsis, thereby amplifying inflammatory cascades through intracellular trafficking pathways[41]. Third, endothelial TLR4 directly mediates cellular response to LPS stimulation, consistent with previous studies showing that TLR4 activation by bacterial products increases endothelial permeability[42]. Together, these findings reveal that TLR4 orchestrates endothelial dysfunction during sepsis through three interconnected pathways: macrophage-mediated inflammation, enhanced endothelial sensitivity to inflammatory signals, and direct endotoxin sensing.

The parallel impairment of both EC and LEC function through these TLR4-dependent pathways represents a critical mechanism in sepsis pathogenesis. While ECs primarily maintain blood-tissue barrier integrity and regulate vascular permeability[8], LECs are essential for interstitial fluid homeostasis and immune cell trafficking through lymphatic vessels[13]. The observed dysfunction of these complementary endothelial populations suggests potential interactions in disease progression: EC damage may contribute to altered vascular permeability and fluid extravasation, while LEC dysfunction could affect fluid homeostasis. Our findings demonstrate that TLR4 signaling contributes to the impairment of both vascular and lymphatic endothelial barriers, providing new insights into endothelial dysfunction in sepsis-induced ALI.

In conclusion, the current study reveals a complex role of TLR4 in orchestrating sepsis-induced ALI through multiple cellular and molecular mechanisms. We demonstrate that TLR4 regulates macrophage function through three distinct yet interrelated pathways: metabolic reprogramming, cholesterol efflux, and inflammatory signaling. In parallel, TLR4 mediates endothelial dysfunction via three interconnected mechanisms: (1) TLR4 on macrophages mediates the production of inflammatory signals that induce endothelial injury; (2) TLR4 on ECs/LECs functions as a critical sensor that determines their susceptibility to macrophage-derived inflammatory mediators; and (3) endothelial TLR4 directly mediates cellular response to endotoxin stimulation. The identification of these mechanistic pathways not only advances our understanding of sepsis pathogenesis but also suggests that targeting TLR4 could provide therapeutic benefits through multiple cellular mechanisms.

While scRNA-seq provided valuable insights into cellular heterogeneity and TLR4-dependent responses during sepsis-induced ALI, we acknowledge certain limitations of the study. It is noticeable that the scRNA-seq data showed a relatively lower proportion of neutrophils than direct neutrophil counts in septic lung tissue under the microscope. This is mainly because scRNA-seq only captures viable neutrophils with intact transcripts instead of total neutrophils, which include neutrophils in different death statuses. Future studies utilizing complementary approaches, such as flow cytometry or spatial transcriptomics, may provide additional insights into neutrophil dynamics and their interaction with other cell types during sepsis-induced ALI. Nevertheless, the current findings highlight the complex cellular and molecular mechanisms through which TLR4 orchestrates sepsis-induced ALI, providing a foundation for future therapeutic strategies.

Materials and methods

Animal strains

Animal procedures were approved by the Institutional Animal Care and Use Committees (IACUC) at University of Pittsburgh and VA Pittsburgh Healthcare System. Male C57BL/6 wild-type (WT) mice, aged 8-10 weeks, were acquired from Jackson Laboratories, while *Tlr4*$^{-/-}$ mice were sourced from the University of Pittsburgh. All mice were housed in specific pathogen-free (SPF) conditions, with 22-25 °C, 50-60% humidity, and 12 h light/dark cycle. Mice were provided with free access to food and water and acclimated for 1 week before experiments.

CLP model

For this procedure, mice were anesthetized via intraperitoneal ketamine (50 mg/kg) and xylazine (5 mg/kg). Through a 1 cm abdominal incision, the cecum was exposed and ligated with 4-0 silk sutures. A single through-and-through puncture was made using a 22-gauge needle. The cecum was returned and the incision closed with 4-0 silk sutures. As per experimental design, mice were euthanized at 24 hours post-CLP for collection of blood, BALF, and lung tissues.

Survival analysis

Survival was monitored for 96 h in WT and *Tlr4*$^{-/-}$ mice after sham or CLP surgery. Each group consisted of 10 male mice (n = 10/group). Kaplan-Meier survival analysis was conducted to compare survival rates between the groups. Mice were observed at regular intervals to ensure continuous and accurate monitoring. Differences in survival curves were assessed using the Log-rank test, with statistical significance defined as $p < 0.05$.

Cell isolation, sorting, and culture

Primary macrophages were isolated from mouse BALF. After anesthesia, mice were intubated (22 G catheter) and lavaged five times with 1 mL ice-cold phosphate-buffered saline (PBS). BALF was centrifuged (300 g, 4 °C, 10 minutes), cells resuspended in PBS and incubated with anti-F4/80 antibody beads (BD Biosciences) at 4°C for 15 minutes. Macrophages were isolated using OctoMACS™ Separator and MS Columns (Miltenyi).

For pulmonary vascular/lymphatic endothelial cell isolation, mouse lungs were minced (~1 mm^3) and digested with 0.2% collagenase I in Hank's balanced salt solution at 37 °C for 45 minutes. The cell suspension was filtered through a 70 μm strainer and centrifuged (300 g, 5 minutes). Cells were incubated with anti-CD31 beads (BD Biosciences) at 4°C for 15 minutes and separated using MS columns. $CD31^+$ cells were cultured in MEMD-Val medium (Invitrogen) with 2 mM glutamine, 10% fetal bovine serum, and 5% human serum (37 °C, 5% CO_2). At 80-90% confluence, cells were incubated with anti-podoplanin antibody (LifeSpan) at 4 °C for 20 minutes, followed by magnetic bead separation. The $CD31^+$/$podoplanin^+$ cells were identified and cultured as LECs, while $CD31^+$/$podoplanin^-$ cells were identified and cultured as vascular ECs under the same conditions.

Purity of the isolated cells was assessed using flow cytometry, ensuring at least 90% purity before proceeding with subsequent experiments (Supplementary Fig. 4A, B).

Western blot analysis

Proteins were extracted using RIPA lysis buffer with protease inhibitors (Sigma), and concentrations were measured with a BCA assay kit (ThermoFisher). For SDS-PAGE, 30 μg of total protein per sample was loaded onto 8% or 10% gels, separated, and transferred to PVDF membranes (Millipore, USA). Membranes were blocked with 5% non-fat milk for one hour at room temperature, then incubated overnight at 4 °C with primary antibodies, including TLR4, ZO-1, Occludin, β-actin, and GAPDH (details in Supplementary Table 1). After HRP-conjugated secondary antibody incubation, protein bands were visualized with enhanced chemiluminescence and imaged using a ChemiDoc system (Bio-Rad).

Hematoxylin and eosin (H&E) staining and lung injury scoring

Lung samples were fixed in 10% neutral buffered formalin, embedded in paraffin, and sectioned into 5 μm slices for H&E staining following standard histopathological procedures. Histopathological changes were observed under a light microscope, and lung injury was assessed in six sections from the lower lobes. Injury criteria included atelectasis, alveolar and interstitial inflammation, hemorrhage, edema, necrosis, and overdistension. Scoring was based on the injury extent: 0 (none), 1 (≤ 25%), 2 (≤ 50%), 3 (≤ 75%), and 4 (diffuse). Blinded pathologists independently evaluated the lung injury scores.

Immunofluorescence staining

Cells or tissues were fixed with 4% paraformaldehyde for 20 minutes, permeabilized with 0.1% Triton X-100 for 10 minutes, and blocked with 5% bovine serum albumin (BSA) for 30 minutes, all at room temperature.

Depending on the specific experiment, primary antibodies against TLR4, F4/80, or ABCA1 were applied for overnight incubation at 4 °C. The following day, samples were incubated with fluorescent secondary antibodies (1:100) in the dark for one hour, and nuclei were stained with DAPI for 5 minutes. Samples were imaged using a Nikon A1R confocal microscope.

Evans blue measurement

To assess mice lung microvascular permeability, Evans blue dye (20 mg/kg, Sigma) was administered intravenously 30 minutes prior to euthanasia. After PBS perfusion to clear intravascular dye, the harvested lungs were homogenized and incubated overnight with 16.7% formamide at 37 °C. The filtered homogenate (70 μm mesh) was analyzed spectrophotometrically at 620 nm and 740 nm. Evans blue extravasation was quantified using a standard curve and expressed as μg Evans blue dye (EBD)/g lung tissue[43].

scRNA-seq workflow

Twenty-four hours post-surgery, lung tissues were harvested from Sham- or CLP-treated *Tlr4*$^{-/-}$ mice. The tissues were washed twice with ice-cold PBS containing 0.04% BSA under sterile conditions and mechanically dissociated into ~0.5 mm^3 fragments. Tissue fragments underwent enzymatic digestion at 37 °C for 30 minutes with periodic agitation at 10-minute intervals. The resulting cell suspension was filtered twice through 70 μm strainers and centrifuged (400 g, 5 minutes, 4 °C). The pellet was resuspended and treated with red blood cell lysis buffer at 4 °C for 5 minutes, followed by two wash-centrifugation cycles (400 g, 5 minutes, 4 °C). The final cell pellet was resuspended in 100 μl medium and adjusted to 30,000 cells per sample. The scRNA-seq libraries were prepared using the 10x Genomics Chromium Next GEM Single Cell 3' Reagent Kit v3.1 following manufacturer's instructions and sequenced on a NovaSeq 6000 platform using high-throughput settings.

scRNA-seq data processing

The scRNA-seq data were processed with Cell Ranger (v5.0.0) to generate gene count matrices. In this study, we sequenced lung cells from *Tlr4*$^{-/-}$ mice subjected to sham or CLP surgery, and integrated these data with publicly available scRNA-seq datasets from WT Sham and WT CLP mice obtained from the GEO database (GSE278767). Quality control retained cells expressing 500-7000 unique genes, fewer than 50,000 total RNA counts, and less than 10% mitochondrial genes. Data analysis was performed with Seurat (v5.0.3)[44], incorporating the Harmony algorithm to correct for batch effects[45]. Cells were then clustered using UMAP with dimensions 1 to 18 and a resolution of 0.3.

Milo and differential abundance analysis

To test changes in cell abundance across different groups at high resolution, we performed differential abundance analysis using Milo, a statistical framework that identifies differences by assigning cells to partially overlapping neighborhoods on a KNN graph[21]. Specifically, we used the "buildGraph" and "makeNhoods" functions with parameters: "k = 30", "d = 50", "prop = 0.2", and "refined = TRUE". Other parameters were chosen based on recommended Milo standards. Differential neighborhood abundance testing was conducted using the "testNhoods" function on the samples.

Differential expression and gene set enrichment analysis

Differential gene expression analysis was conducted using the "FindMarkers" function, with criteria set to P-value < 0.005 and $Log_2FC > 0.585$. To investigate the functional mechanisms underlying the differences between groups, Gene Ontology (GO) and Kyoto Encyclopedia of Genes and Genomes (KEGG) pathway enrichment analyses were performed using the "enrichGO" and "enrichKEGG" functions to identify biological pathways associated with DEGs.

AUCell analysis for pathway enrichment scores

To calculate enrichment scores for inflammatory response, positive ROS, glycolysis, OXPHOS, lipid metabolism, and cholesterol efflux in single-cell data, we performed AUCell analysis[46]. Relevant gene sets were obtained from the Molecular Signatures Database (http://www.gsea-msigdb.org/gsea/msigdb/index.jsp), and scores were computed using AUCell based on these gene sets.

Evaluation of mitochondrial membrane potential

Mitochondrial membrane potential was assessed using JC-1 staining, with Hoechst 33342 for nuclear counterstaining. After a 20-minute incubation at 37 °C and subsequent media washing, cells were imaged by confocal microscopy with a 60× objective. Under normal mitochondrial membrane potential, JC-1 forms aggregates, emitting red fluorescence; when membrane potential decreases, JC-1 shifts to monomers, emitting green fluorescence, indicative of mitochondrial damage.

Cholesterol efflux assay

Cholesterol efflux was measured using a fluorescence-based assay kit (ab196985, Abcam). In brief, macrophages (1×10^5) were labeled with cholesterol for 1 hour, followed by overnight incubation in Equilibration Buffer. Cells were then exposed to the cholesterol acceptor (serum) for 6 hours at 37 °C with 5% CO_2. Fluorescence intensity was measured in both the media and cell lysates using a microplate reader (Ex/Em = 482/515 nm). Cholesterol efflux was calculated as the ratio of fluorescence intensity in the media to the total fluorescence intensity (media + cell lysate).

Cell communication analysis

Intercellular communication networks were analyzed using the CellChat package[47]. Following CellChat object creation, communication probabilities and L-R interactions were computed, with significant interactions defined as L-R pairs with $P < 0.05$ between cell populations.

Transwell co-culture setup

For co-culture experiments, ECs or LECs (2×10^4 cells/well) were seeded on the upper chamber of 0.4 μm pore size Transwell inserts (Corning Costar) and cultured until confluence. Macrophages (1×10^5 cells/well) isolated from Sham or CLP mice were placed in the bottom chamber. The co-culture system was maintained in MEMD-Val complete medium at 37 °C with 5% CO_2. After 24 hours of co-culture, ECs/LECs were harvested for subsequent analyses.

Apoptosis analysis

Apoptosis was assessed using the Annexin V-FITC Apoptosis Detection Kit (ThermoFisher, USA). Cells were stained with Annexin V-FITC and propidium iodide according to manufacturer's instructions and analyzed by flow cytometry (LSRFortessa, BD Biosciences). Data analysis was performed using FlowJo software (v10, USA).

Statistical analysis

Data analysis was performed using R Studio (v4.3.3) and Graphpad Prism (v9.5). Results are presented as mean ± SD from at least three independent experiments. Survival analysis was conducted using the Kaplan-Meier method with log-rank test. Statistical comparisons were made using Student's t-test (two groups) or two-way ANOVA followed by Bonferroni's post-hoc test (factorial design with two variables), with significance set at $P < 0.05$.

Reporting summary

Further information on research design is available in the Nature Portfolio Reporting Summary linked to this article.

Data availability

The source data for the graphs and charts in the main figures are provided in Supplementary Data. Uncropped original blot/gel images from the main figures are available in Supplementary Fig. 5. The scRNA-seq data have been deposited in the GSE287641. All other data can be obtained from the corresponding author upon reasonable request.

Code availability

This study did not develop custom computer code. All analyses were performed following standard protocols for single-cell data processing in R Studio (v4.3.3) with main packages including Seurat (v5.0.3), miloR (v2.2.0), AUCell (v1.28.0), and CellChat (v2.1.0). The complete code used for data processing and analysis can be obtained from the corresponding author upon reasonable request.

Received: 19 November 2024; Accepted: 11 March 2025;
Published online: 21 March 2025

References

1. Singer, M. et al. The third international consensus definitions for sepsis and septic shock (sepsis-3). *JAMA* **315**, 801–810 (2016).
2. Xie, J. et al. The epidemiology of sepsis in Chinese ICUs: a national cross-sectional survey. *Crit. Care Med.* **48**, e209–e218 (2020).
3. Genga, K. R. & Russell, J. A. Update of sepsis in the intensive care unit. *J. Innate Immun.* **9**, 441–455 (2017).
4. Kumar, V. Pulmonary innate immune response determines the outcome of inflammation during pneumonia and sepsis-associated acute lung injury. *Front. Immunol.* **11**, 1722 (2020).
5. Tomazini, B. M. et al. Effect of dexamethasone on days alive and ventilator-free in patients with moderate or severe acute respiratory distress syndrome and COVID-19: the CoDEX randomized clinical trial. *JAMA* **324**, 1307–1316 (2020).
6. Meyer, N. J., Gattinoni, L. & Calfee, C. S. Acute respiratory distress syndrome. *Lancet***398**, 622–637 (2021).
7. Gorman, E. A., O'Kane, C. M. & McAuley, D. F. Acute respiratory distress syndrome in adults: diagnosis, outcomes, long-term sequelae, and management. *Lancet***400**, 1157–1170 (2022).
8. Joffre, J., Hellman, J., Ince, C. & Ait-Oufella, H. Endothelial responses in sepsis. *Am. J. Respir. Crit. Care Med.* **202**, 361–370 (2020).
9. Dolmatova, E. V., Wang, K., Mandavilli, R. & Griendling, K. K. The effects of sepsis on endothelium and clinical implications. *Cardiovasc. Res.* **117**, 60–73 (2021).
10. Qiao, X., Yin, J., Zheng, Z., Li, L. & Feng, X. Endothelial cell dynamics in sepsis-induced acute lung injury and acute respiratory distress syndrome: pathogenesis and therapeutic implications. *Cell Commun. Signal.***22**, 241 (2024).
11. Breslin, J. W. Edema and lymphatic clearance: molecular mechanisms and ongoing challenges. *Clin. Sci.***137**, 1451–1476 (2023).
12. Stump, B., Cui, Y., Kidambi, P., Lamattina, A. M. & El-Chemaly, S. Lymphatic changes in respiratory diseases: more than just remodeling of the lung? *Am. J. Respir. Cell Mol. Biol.* **57**, 272–279 (2017).
13. Reed, H. O. et al. Lymphatic impairment leads to pulmonary tertiary lymphoid organ formation and alveolar damage. *J. Clin. Investig.* **129**, 2514–2526 (2019).
14. Hattori, Y., Hattori, K., Machida, T. & Matsuda, N. Vascular endotheliitis associated with infections: its pathogenetic role and therapeutic implication. *Biochem. Pharmacol.* **197**, 114909 (2022).
15. Kang, S. & Kishimoto, T. Interplay between interleukin-6 signaling and the vascular endothelium in cytokine storms. *Exp. Mol. Med.* **53**, 1116–1123 (2021).
16. Poyomtip, T. Roles of toll-like receptor 4 for cellular pathogenesis in primary open-angle glaucoma: a potential therapeutic strategy. *J. Microbiol. Immunol. Infect.***52**, 201–206 (2019).
17. Park, B. S. & Lee, J. O. Recognition of lipopolysaccharide pattern by TLR4 complexes. *Exp. Mol. Med.* **45**, e66 (2013).
18. Deravi, N. et al. The Yin and Yang of toll-like receptors in endothelial dysfunction. *Int. Immunopharmacol.* **108**, 108768 (2022).
19. Khakpour, S., Wilhelmsen, K. & Hellman, J. Vascular endothelial cell Toll-like receptor pathways in sepsis. *Innate Immun.* **21**, 827–846 (2015).
20. Gong, T. et al. Decoding the multiple functions of ZBP1 in the mechanism of sepsis-induced acute lung injury. *Commun. Biol.* **7**, 1361 (2024).
21. Dann, E., Henderson, N. C., Teichmann, S. A., Morgan, M. D. & Marioni, J. C. Differential abundance testing on single-cell data using k-nearest neighbor graphs. *Nat. Biotechnol.* **40**, 245–253 (2022).
22. Puleston, D. J. et al. Polyamines and eIF5A hypusination modulate mitochondrial respiration and macrophage activation. *Cell Metab.* **30**, 352–363.e358 (2019).
23. Pérez, S. & Rius-Pérez, S. Macrophage polarization and reprogramming in acute inflammation: a redox perspective. *Antioxidants* **11**, https://doi.org/10.3390/antiox11071394 (2022).
24. Wang, F. et al. Interferon gamma induces reversible metabolic reprogramming of M1 macrophages to sustain cell viability and pro-inflammatory activity. *EBioMedicine* **30**, 303–316 (2018).
25. Wang, F. et al. Glycolytic stimulation is not a requirement for M2 macrophage differentiation. *Cell Metab.* **28**, 463–475.e464 (2018).
26. Zhang, J. et al. ABCA1 deficiency-mediated glomerular cholesterol accumulation exacerbates glomerular endothelial injury and dysfunction in diabetic kidney disease. *Metab. Clin. Exp.* **139**, 155377 (2023).
27. Minanni, C. A. et al. Persistent effect of advanced glycated albumin driving inflammation and disturbances in cholesterol efflux in macrophages. *Nutrients* **13**, https://doi.org/10.3390/nu13103633 (2021).
28. Li, Y. et al. Qing-Xue-Xiao-Zhi formula attenuates atherosclerosis by inhibiting macrophage lipid accumulation and inflammatory response via TLR4/MyD88/NF-κB pathway regulation. *Phytomedicine***93**, 153812 (2021).
29. Sun, M. et al. BIG1 mediates sepsis-induced lung injury by modulating lipid raft-dependent macrophage inflammatory responses. *Acta Biochim. Biophys. Sin.* **53**, 1088–1097 (2021).
30. Gualandris, A. et al. Role of TGFβ1 and WNT6 in FGF2 and BMP4-driven endothelial differentiation of murine embryonic stem cells. *Angiogenesis* **25**, 113–128 (2022).
31. Han, B. et al. Integrating spatial and single-cell transcriptomics to characterize the molecular and cellular architecture of the ischemic mouse brain. *Sci. Transl. Med.* **16**, eadg1323 (2024).
32. Yang, X. et al. Bacterial endotoxin activates the coagulation cascade through gasdermin D-dependent phosphatidylserine exposure. *Immunity* **51**, 983–996.e986 (2019).
33. Ratitong, B., Marshall, M. & Pearlman, E. β-Glucan-stimulated neutrophil secretion of IL-1α is independent of GSDMD and mediated through extracellular vesicles. *Cell Rep.* **35**, 109139 (2021).
34. Palsson-McDermott, E. M. et al. Pyruvate kinase M2 regulates Hif-1α activity and IL-1β induction and is a critical determinant of the warburg effect in LPS-activated macrophages. *Cell Metab.* **21**, 65–80 (2015).
35. Mills, E. L. et al. Succinate dehydrogenase supports metabolic repurposing of mitochondria to drive inflammatory macrophages. *Cell* **167**, 457–470.e413 (2016).
36. Liu, L. et al. Proinflammatory signal suppresses proliferation and shifts macrophage metabolism from Myc-dependent to HIF1α-dependent. *Proc. Natl. Acad. Sci. USA* **113**, 1564–1569 (2016).
37. Amunugama, K., Pike, D. P. & Ford, D. A. The lipid biology of sepsis. *J. Lipid Res.* **62**, 100090 (2021).
38. Yvan-Charvet, L. et al. Increased inflammatory gene expression in ABC transporter-deficient macrophages: free cholesterol accumulation, increased signaling via toll-like receptors, and neutrophil infiltration of atherosclerotic lesions. *Circulation* **118**, 1837–1847 (2008).
39. Zhu, X. et al. Macrophage ABCA1 reduces MyD88-dependent Toll-like receptor trafficking to lipid rafts by reduction of lipid raft cholesterol. *J. Lipid Res.* **51**, 3196–3206 (2010).
40. Zhang, X. et al. Effects of caprylic acid and eicosapentaenoic acid on lipids, inflammatory levels, and the JAK2/STAT3 pathway in ABCA1-

deficient mice and ABCA1 knock-down RAW264.7 cells. *Nutrients* **15**, https://doi.org/10.3390/nu15051296 (2023).
41. Gong, T. et al. Mechanism of lactic acidemia-promoted pulmonary endothelial cells death in sepsis: role for CIRP-ZBP1-PANoptosis pathway. *Mil. Med. Res.* **11**, 71 (2024).
42. Gong, P. et al. TLR4 signaling is coupled to SRC family kinase activation, tyrosine phosphorylation of zonula adherens proteins, and opening of the paracellular pathway in human lung microvascular endothelia. *J. Biol. Chem.* **283**, 13437–13449 (2008).
43. Burkard, P. et al. A key role for platelet GPVI in neutrophil recruitment, migration, and NETosis in the early stages of acute lung injury. *Blood* **142**, 1463–1477 (2023).
44. Hao, Y. et al. Dictionary learning for integrative, multimodal and scalable single-cell analysis. *Nat. Biotechnol.* **42**, 293–304 (2024).
45. Korsunsky, I. et al. Fast, sensitive and accurate integration of single-cell data with Harmony. *Nat. Methods* **16**, 1289–1296 (2019).
46. Aibar, S. et al. SCENIC: single-cell regulatory network inference and clustering. *Nat. Methods* **14**, 1083–1086 (2017).
47. Jin, S. et al. Inference and analysis of cell-cell communication using CellChat. *Nat. Commun.* **12**, 1088 (2021).

Acknowledgements

We thank Chaowei Shang, Ph.D., Director of Microscopy Facility at University of Pittsburgh for assistance with confocal microscopy and immunofluorescence. This work was supported by the US National Institutes of Health Grant R21AI185275 (J.F.), US Department of Veterans Affairs Award 1I01BX004838 (J.F.) and IK6BX006297 (J.F.).

Author contributions

All authors contributed to the study conception and design. Material and animal preparation, data collection, and analysis were performed by Y.F., T.G., P.A.L., and Y.H.L.; Y.F., Z.M.W., T.R.B., Y.T.L., and J.F. planned the project and conceived the experiments. Y.F., T.G., and J.F. wrote the manuscript. All authors approved the final manuscript.

Competing interests

The authors declare no competing interests.

Additional information

Supplementary information The online version contains supplementary material available at https://doi.org/10.1038/s42003-025-07921-3.

Correspondence and requests for materials should be addressed to Jie Fan.

Peer review information *Communications Biology* thanks Monowar Aziz and Lin Zou for their contribution to the peer review of this work. Primary Handling Editors: Christopher LaRock and Mengtan Xing.